Sources for constellation errors in modulated dispersion interferometers

K. J. Brunner, J. Knauer, J. Meineke, et al.

View Online   Export Citation   CrossMark

ARTICLES YOU MAY BE INTERESTED IN

Sources for constellation errors in modulated dispersion interferometers

View Online   Export Citation   CrossMark

K. J. Brunner,[1,a)] J. Knauer,[1] J. Meineke,[1] H. I. Cu Castillo,[2,b)] M. Hirsch,[1] B. Kursinski,[1] M. Stern,[1] R. C. Wolf,[1] and W7-X Team[c)]

AFFILIATIONS

[1] Max-Planck-Institute for Plasma Physics, Wendelsteinstr. 1, 17489 Greifswald, Germany
[2] Universidad Autónoma de Yucatán, Calle 60 491A, 97000 Mérida, Yucatan, Mexico

[a)]Author to whom correspondence should be addressed: k.j.brunner@ipp.mpg.de
[b)]Also at: Max-Planck-Institute for Plasma Physics, Greifswald, Germany.
[c)]For a full list of contributors, see T. Klinger *et al.*, Nucl. Fusion **59**, 112004 (2019).

ABSTRACT

Dispersion interferometry (DI) is being employed on an increasing number of fusion experiments to measure the plasma density with a minimal sensitivity to vibrations. DIs employed in high-density experiments use phase modulation techniques up to several hundred kilohertz to enable quadrature detection and to be unaffected by variations of the signal amplitude. However, the evaluation of the temporal interferogram can be a significant source for phase errors and does not have an established processing method. There are two non-approximation-based methods currently in use: one using the ratio of amplitudes in the signal's Fourier spectrum and the other using its sectioned integration. Previously, the methods could not be used simultaneously since they differ in their respective calibration point. In this paper, we present a technique to use both phase evaluation methods simultaneously using quadrature correction methods. A comparison of their strengths and weaknesses is presented based on identical measurements indicating one to be more reliable in a more static measurement scenario, while the other excels in highly dynamic ones. Several comparative experiments are presented, which identify a significant error source in the phase measurement induced by polarization rotation. Since the same effect may be induced by Faraday rotation, the results may have direct consequence on the design of the ITER dispersion interferometer/polarimeter as well as the European DEMO's interferometer concept.

I. INTRODUCTION

Interferometry is the primary density control diagnostic for fusion machines in the world.[1–7] The technique's primary advantage is its simplicity. To first order, it is only sensitive to the dispersion of the traversed medium and the wavelength of the employed laser beam. The effect of vibrations on the geometric path length has been mostly eliminated using advanced techniques, such as dispersion interferometry (DI) or the well-established two-color interferometry. For these reasons, even future large-scale machines plan to use interferometry for real-time density control.[8,9] On large-scale machines achieving significant plasma densities, e.g., the Joint European Torus (JET) or Wendelstein 7-X (W7-X), interferometers employ phase modulation to handle the phase ambiguity occurring at phase shifts larger than π.[2,6] The modulation scheme can

vary between different types of interferometers, but ultimately the phase information is always moved into the time domain, making the scheme impervious to changes in the signal amplitude as long as they are outside of the modulation-frequency time domain.

A dispersion interferometer (DI) is a diagnostic variant of the interferometer principle, which employs frequency doubling crystals (FDC) to create collinear coherent beams of differing wavelength.[10] This in turn results in highly efficient compensation of phase changes induced by geometric path length changes. This is something that a two-color interferometer can only achieve with extremely good alignment. However, this benefit comes at a disadvantage: DIs rely on the nonlinear process of frequency doubling. The wavelengths chosen in large-scale DIs are often in the 4–11 μm range, which offers a compromise of sensitivity, refraction resilience, and susceptibility to surface erosion of the plasma facing mirror.

The latter is significantly higher in the Nd:YAG wavelength range around 1 μm.[11] In these wavelength ranges, frequency doubling is highly inefficient requiring well over 10 W of pump power for a milliwatt of the doubled signal due to the low nonlinear coefficient of the materials involved.[12]

Currently, the evaluation of a DI's temporal interferogram is being done using two analytically derived methods. The first was developed at the Large Helical Device (LHD) using a lock-in amplification-based method and the second at W7-X using direct integration on a Field Programmable Gate Array (FPGA).[6,13] An additional method was used at the TEXTOR experiment, which since then has been abandoned as it has difficulties with low signal levels commonly found in larger experiments as well as exhibiting an amplitude dependence.[14] In consequence, this method will not be addressed here. As will be discussed in Sec. II, both methods currently in use differ in their operating point and have therefore not been used together. In this paper, we present a method to combine both phase evaluation methods using quadrature correction schemes. This enables their direct comparison using the same optical setup and measurements, thus showing their applicability to various measurement scenarios.

In the past, both of the methods currently in use have reported significant non-linearities in their phase response resulting in measurement errors.[3,6] The errors could measure up to 0.6 rad at W7-X, which dominated the phase error for the interferometer. An investigation into the source of these phase errors was not conducted so far. By combining the phase evaluation methods, we could identify major sources for constellation errors. The first is related to the placement of the modulator and can be mitigated by minor adjustments of the optical layout. The second is related to the orientation of the FDCs and affects both phase evaluation methods. While this can be mitigated for currently operating systems, it may pose a significant source of error for future large scale DIs measuring under the effect of significant plasma-induced Faraday rotation, as will be discussed in Sec. VI. In addition, the simultaneous usage of the method revealed an apparent amplitude dependence in the integration-based method.

In Sec. II, the mathematical fundamentals important for the understanding of the presented work will be reviewed, including a short description of the implementation of the processing techniques used in the remaining sections. This is followed by a description of the method for combining the two aforementioned phase extraction algorithms in Sec. III. Section IV presents the results of laboratory experiments identifying previously unknown phase errors using the combination of methods. In Sec. V, the measurement of a W7-X discharged is used to compare the two phase extraction methods' performance in a realistic measurement scenario. Finally, the results of the experiments presented are discussed and put into context of future fusion devices, such as ITER and DEMO, in Sec. VI.

II. BACKGROUND

For the sake of brevity, this report will not re-iterate the working principle of a DI. Akiyama *et al.* very well describe this in a recent review article.[10] Similarly, the phase evaluation methods are only re-iterated where it is necessary for the understanding of the paper.

For a thorough derivation of the respective methods, the reader is referred to the respective diagnostic papers.[6,13]

To recapitulate, the diode signal I_{sig} of a phase-modulated DI can be described as

$$I_{sig} = \underbrace{I_1 + I_2}_{DC\ component} + \underbrace{2\sqrt{I_1 I_2}\cos(\rho\sin(\omega_m t) + \phi_p)}_{component\ with\ phase\ information}, \qquad (1)$$

where $I_{1,2}$ denote the intensity of the second harmonic beam generated by the first and second FDC, respectively. The measured phase ϕ_p is ideally only affected by the dispersive medium under investigation, e.g., the plasma. The diode signal is phase modulated at the frequency ω_m and an amplitude ρ, generating a periodic diode signal, as shown in Fig. 1. The in-phase (I) and quadrature (Q) components are generated from the right-hand part of the diode signal. The method by Akiyama *et al.* uses a lock-in amplifier (LIA), which extracts the amplitude of the first and second harmonic of the diode signal's spectrum, yielding

$$\begin{aligned} I_{LIA} &\propto J_2(\rho)\cos(\Phi_P + \Phi_0), \\ Q_{LIA} &\propto -J_1(\rho)\sin(\Phi_P + \Phi_0). \end{aligned} \qquad (2)$$

In Eq. (2), the components are modified by Bessel functions $J_n(\rho)$ of nth order. The method requires both an input and an output filter to extract the frequency components,[15] which reduces the available bandwidth of the measured phase as well as introducing phase delay and pulse elongation. The method developed at W7-X, on the other hand, directly integrates the diode signal shown in the top of Fig. 1 after removing the DC component from Eq. (1). By summation of the partial integrals the I and Q components can be generated as

$$\begin{aligned} I_{int} &\propto J_0(\rho)\cos(\Phi_P + \Phi_0), \\ Q_{int} &\propto -H_0(\rho)\sin(\Phi_P + \Phi_0). \end{aligned} \qquad (3)$$
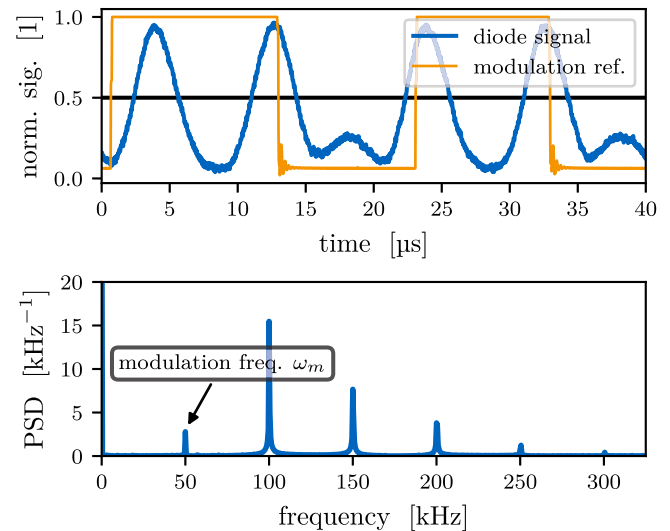
FIG. 1. An example for a modulated DI's signal. The temporal interferogram as measured by the diode is shown in thick blue on the top and the modulator's reference signal in thin orange. The bottom shows the spectral composition of the diode signal shown at the top.

In Eq. (3), the quadrature component is modified by the Struve function of 0th order $H_0(\rho)$, which is a Bessel-type function solving the non-homogeneous Bessel differential equation. No output filter is applied in this method, as the integration itself acts as an anti-aliasing filter. This preserves significantly more bandwidth in the output signal. The input signal does require the digital removal of the diode signal's DC component shown in Eq. (1), which is done using an averaging min–max filter. This is a type of nonlinear filter, which preserves the DC component of the right addend in Eq. (1). It uses the maximum and minimum detected during a modulation period and subtracts the median from the values of the respective modulation period to extract the right addend of Eq. (1). Since this type of filter is very susceptible to noise, the detected minima and maxima are averaged over multiple periods.

The desired plasma phase Φ_P can be acquired by taking the four-quadrant arcus-tangent and subtracting the zero-phase Φ_0, i.e., $\Phi_P = \arctan2(I/Q) - \Phi_0$, assuming that I and Q are placed on a circle. The latter is only true if the modulation depth ρ is chosen such that $J_2(\rho) = -J_1(\rho)$ or $J_0(\rho) = -H_0(\rho)$, respectively. The modulator defines the modulation depth. In most cases, it can be varied and while it is simple to derive the analytic ρ necessary to match both components, real systems require some calibration because the modulator is usually passed at an oblique angle or off-center in a double-pass.

A. Implementation

Both methods described above were implemented using Python. The integration-based method (IM) was implemented as described by the original publication in single-data rate mode.[6] Integration is, hence, conducted numerically from the rising edge of the reference signal to the next rising edge, using the falling edge as an inversion point for the accumulator. The only modification to the original implementation is the averaging in the extrema detected by the min–max filter. For this work, the filter averages over 1000 periods to reduce the effect of noise.

The LIA-based method (LM) was implemented in Python using a digital LIA. First, a phase-locked loop (PLL) generates two sine reference signals using a direct look-up table (DLT) approach:[16] One is at the modulation frequency, while the other is at the second harmonic. These are then multiplied with the band-pass filtered diode signal. The resulting down-mixed signals are low-pass filtered to generate the in-phase and quadrature components.[15] This implementation is a standard method applicable to a micro-controller based design and is equivalent to the implementation by Akiyama *et al.*

III. SIMULTANEOUS CALIBRATION OF DI PHASE EVALUATION METHODS

For either method, calibration is conducted using a wedge placed in the beam path, as shown in Fig. 2. For the experiments conducted in this paper, the wedge is made from ZnSe. The wedge can be moved perpendicular to the beam using a brush-less DC motor, thus introducing a phase shift between the 10.6 μm pump beam and the 5.3 μm beam generated by the first FDC. In this way, a phase shift from 0 to 2π can be scanned, and a constellation diagram is generated. By comparing the measured phase over the drive
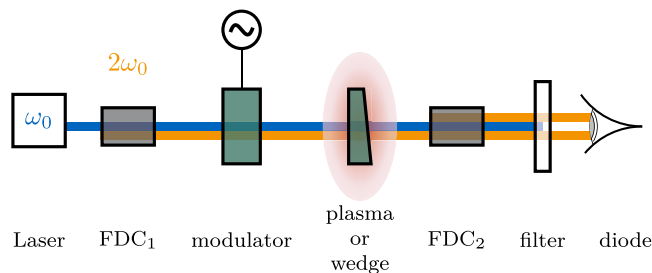
FIG. 2. The basic setup of a dispersion interferometer with a calibration wedge.

region with constant speed to a linear regression fit, the constellation error σ_c, i.e., the error due to the "non-circularity" of the constellation, can be estimated yielding the maximum systematic error of the interferometer for a particular value of ρ. By scanning ρ, an optimum modulation depth for a given optical setup can be found. This method has previously been described for the IM at W7-X,[6] but works equally well for the LM, with the caveat that the optimal ρ differs between the methods.

A. I/Q correction

The calibration-relevant functions defining the I and Q components are plotted in Fig. 3. Figure 3(a) shows the components of Eq. (2) and Fig. 3(b) the ones of Eq. (3). As indicated, calibration requires, for example, $J_0(\rho_{\mathrm{opt}}) = -H_0(\rho_{\mathrm{opt}})$. As mentioned in Sec. II, the analytical value of ρ_{opt} can be found easily but may differ from the experimentally found value. For the remainder of the work presented, we arbitrarily choose ρ to optimize the IM, which makes drawing parallels to W7-X experiments easier. This is indicated in Fig. 3. This particular choice of ρ_{opt} leads to an imbalance in the LIA-method's I/Q components. To numerically calibrate the LM, it is necessary to scale the Q_{LIA} component to match its respective
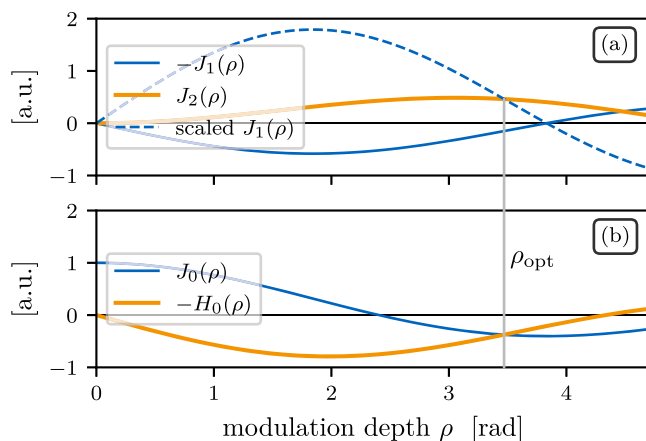
FIG. 3. A plot of the calibration-relevant functions for Eq. (2) in (a) and for Eq. (3) in (b). The dashed line is the scaled J_1-function to match J_2 at the indicated value ρ_{opt}. The range of ρ-values depicted is roughly the available range available in the experiments presented here.
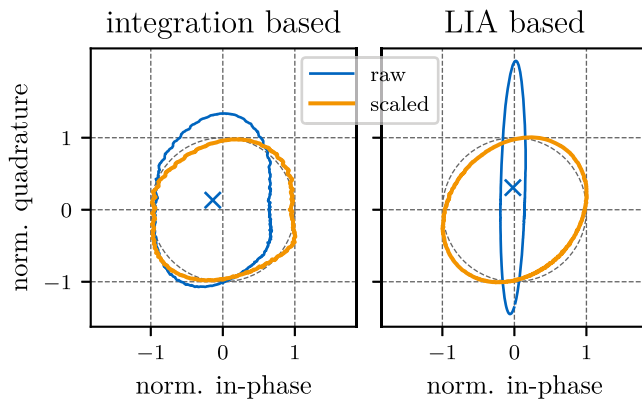
FIG. 4. Example of a basic I/Q correction applied to the dispersion interferometer constellation for both the integration-based (left) and LIA-based (right) phase evaluation methods.

in-phase component, i.e., by analytically doing $J_{1,\text{scaled}}(\rho) = J_1(\rho) \cdot \frac{J_2(\rho_{\text{opt}})}{J_1(\rho_{\text{opt}})}$. This is shown by the dashed line in Fig. 3(a).

From Eqs. (2) and (3), one can predict that using an incorrect ρ for either method would only result in an elongation of the constellation diagram along one of the dimensions. In practice, however, the distortions are much more complex, as depicted in Fig. 4 in thin blue. Here, the left side shows an exemplary constellation for the IM and the right-hand side the one for the LM. The distortions of the integration-based phase evaluation are comparatively complex. The LIA-based approach, on the other hand, exhibits a comparatively simple I/Q distortion, i.e., an elongated and rotated ellipse. Such distortions can usually be described by an offset, an amplitude imbalance, and an angle of rotation and are well known in radio and microwave systems.

However, while the correction of a rotated I/Q ellipse has previously been demonstrated,[17] we do not fully correct it here, since the IM exhibits more complex distortions with an ambiguous rotation angle. Instead, we use the rotation of the ellipse as an indicator for constellation errors in Sec. IV. Hence, we first correct the I/Q offset, which was determined from the average of the data's extrema in I and Q (indicated by the blue × in Fig. 4). After removing the offset, the extrema are normalized to the unit circle as shown. This reduces the measurement error significantly and allows us to use both evaluation methods simultaneously after an appropriate calibration measurement. However, for large rotations of the constellation ellipse, this reduced compensation scheme will undoubtedly perform poorly, as will be shown in Sec. IV B.

Figure 4 shows that the distortions of the (corrected) LIA constellation are much simpler when compared to the compensated constellation of the IM. This is an additional motivation to choose ρ such that it optimizes the IM. While the LM's constellation can be easily corrected using the I/Q correction methods described earlier, the same is not true for the complex shape of the IM.

B. Automated calibration of the modulation depth

To speed up the measurements presented here, an automated calibration routine was developed, which minimizes the error of a phase evaluation method without I/Q correction. The automation is on first sight a matter of a simple gradient descent minimization. However, while this does work reasonably well for the LM, the IM has an additional calibration factor that in itself depends on ρ: the reference signal from the modulator and the diode signal need to be aligned in time. More explicitly, the reference signal needs to be delayed such that the rising edge of the reference signal coincides with the rising edge of the diode signal. For the IM, this is an important calibration factor as the method generates the quadrature components for the ratio of the diode signal's half-period-integrals. Hence, one cannot use a portion of the second half-period and add it to the first half without affecting this ratio. An incorrect reference delay results in a significant distortion of the constellation.

The reference delay is a function of the modulation depth induced by the modulator and, hence, would require another dimension of measurements. To prevent this, we developed a robust approach to find the optimal "reference delay," which generates two synthetic diode signals. These are 180° out of phase from each other. The synthetic signals are locked to the reference signal by a PLL, and hence, the reference delay can be found robustly by cross-correlating them with the wedge measurements. Using a single synthetic signal is insufficient for a robust detection of the reference delay due to the symmetry of the diode signal's half-periods.

The automated reference delay detection enables the optimization of ρ under the effect of constellation errors without having to conduct a number of measurements each time to find the reference delay.

IV. EXPERIMENTAL INVESTIGATION OF CONSTELLATION ERRORS

The simultaneous usage of two distinctly different phase evaluation methods offers the possibility to investigate constellation errors seen at W7-X in previous campaigns.[6] In addition, their performance can be compared in different measurement scenarios in order to see whether one method is to be preferred over the other.

To investigate the errors induced into the dispersion interferometer, a basic DI was built in the laboratory with a setup shown in Fig. 2. AgGaSe$_2$ was chosen as an FDC material.[18] This type of crystal is critically phase-matched. In the setup here, the second-harmonic's DC signal measured after the first FDC was maximized and then maintained. A photo-elastic modulator (PEM), a HINDS I/ZN-50 as employed by LHD and W7-X, was used as a phase modulator. The PEM was anti-reflection coated to prevent internal reflections. The PEM was placed vertically and could be moved both longitudinal and perpendicular to the probing beam. To prevent any reflection effects to affect the measurement, the probing beam passed the PEM at roughly 5° vs the aperture normal. The phase shift was induced by a single wedge placed on a linear stage, which would move perpendicular to the beam and is able to scan over 2π in phase shift. The second FDC could be rotated around the probing beam, thus mixing ordinary (O) and extra-ordinary (X) pump components. In addition, the crystal could be rotated around the vertical to find the phase matching angle and maximize doubling efficiency.

The errors investigated were taken from a wedge scan as described above. All analysis was done in post-processing on a computer using raw data acquired by an FPGA-based digitizer sampling at 50 M sample/s at 14 bits. The digitization hardware used in the

laboratory experiments in Secs. IV A and IV B and the plasma experiments shown in Sec. V were identical.

A. PEM position as error source

From the composition of the deformations of the integration constellation, it was previously established that the error source had to be a PEM-synchronous oscillation on the diode signal.[6] Prior to this work, W7-X employed a double-pass through the PEM. This requires passing the probing beam through the aperture off-axis. However, because the birefringence induced in a PEM is proportional to the stress induced into the glass, which in turn is produced by a standing wave in the glass-body, the modulation depth ρ is non-uniform across the aperture and falls off toward the edges.[19] Because the probing beam has a significant size when passing through the PEM, it was speculated that the ρ-non-uniformity across the probing beam itself was a source for error.

To investigate this, a 2D scan of the PEM was conducted in which the PEM was moved along and perpendicular to the beam in a single-pass layout similar to what is depicted in Fig. 2. At each position, the constellation error σ_c was measured using a wedge scan. The calibration of ρ_c was done prior to the shown measurements with the beam waist at the center of the PEM. Figure 5 shows the results of this error scan. Figure 5(a) shows the beam radius as calculated by ZEMAX for the measurement setup in black, with the sampled z-positions marked by vertical lines. The lasers used in current DIs (and at W7-X) tend to be mono-mode TEM00 CO_2-lasers operating with an m^2-factor of better than 1.3. Hence, the ZEMAX calculation is assumed to be a good approximation for the true beam size. As indicated, the yellow line corresponds roughly to the beam-size used in W7-X during the last operation campaign. Figures 5(b) and 5(c) show the constellation error σ_c moving the PEM perpendicular to the beam trajectory. The solid lines were calculated using the IM, where Fig. 5(b) is measured without the I/Q correction and Fig. 5(c) has it applied. The dashed line in Fig. 5(c) indicates the error measured by the corrected LM. The origin marks the center of the PEM aperture based on the symmetry point of the raw error shown in Fig. 5(b). Using the measured center of the PEM aperture was unreliable here as the localization of the beam in combination with the placement of the PEM had an error of over 1 mm attached to it. The black lines in Figs. 5(b) and 5(c) mark the rough positions of the probing beams during the first three experimental campaigns of W7-X, i.e., the beams going in direction of the plasma and returning from it. They are based on the optical design of the W7-X interferometer system, not the actual measurement.

The measurements in Fig. 5(b) show that σ_c quickly increases as the beam is placed off-center. This happens faster for a large beam. As previously mentioned, the modulation depth ρ is a function of position in the modulator glass, and hence, a quick conclusion is that the effective modulation depth of the beam is reduced as the beam moves away from the center, thus moving away from the calibration point ρ_c. This illustrates why the calibration set-point for ρ differed to the analytical value in the W7-X interferometer.

A reduction in the total ρ averaged over the beam cross section can be compensated by the I/Q correction schemes in Sec. III. This leaves only the effect of a ρ-gradient across the beam as an error source via deformations of the constellation. Figure 5(c) shows the same measurements with I/Q correction applied (solid lines).
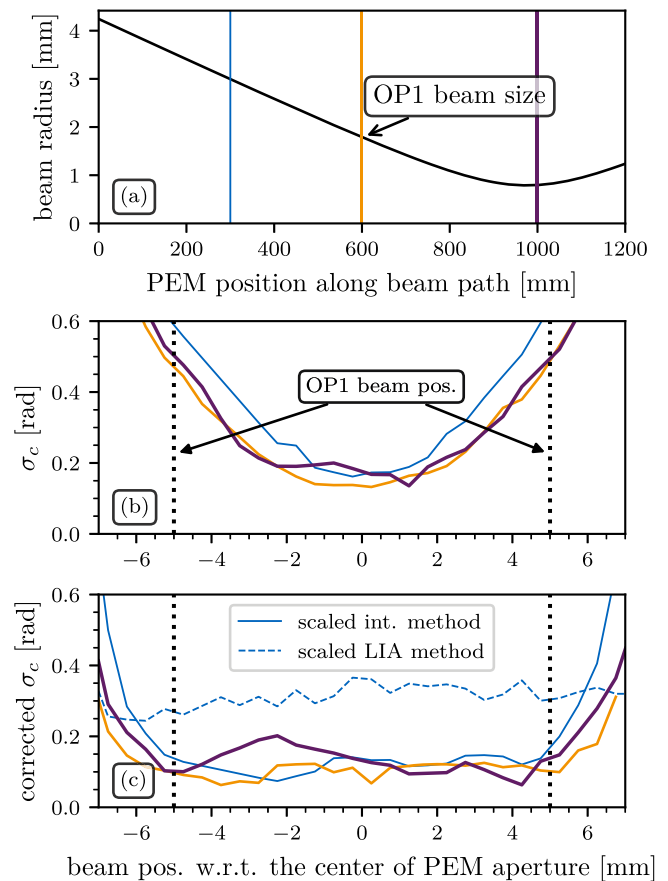
FIG. 5. Constellation error σ_c measured for various positions of the PEM. (a) shows the Gaussian beam radius as calculated by ZEMAX with the vertical lines marking the sampled z-positions. (b) and (c) show the radial scan at each position, with 0 marking the rough center of the PEM aperture ± 1 mm. Each data point is the constellation error σ_c measured by a wedge scan, where (b) plots the σ_c without I/Q correction and (c) with I/Q correction applied. The black dotted vertical lines in (b) and (c) indicate the rough position of the beam in the first three experimental campaigns at W7-X (OP1).

In addition, the σ_c for the corrected LM is plotted for the scan at 300 mm.

The first observation made from the graph is that the total σ_c is reduced with respect to the uncompensated measurements for nearly all positions. The apparent increase in relative noise of the curves shown in Fig. 5(c) can be attributed to the noisy measurements acquired with the lab setup. Nonetheless, it is evident from the graph that the σ_c curve became comparatively flat for most of the PEM's aperture. However, starting at 4 mm from the center, σ_c increases noticeably in the IM. Again, the larger beam of 3 mm is affected closer to the center. As indicated by the black lines, the W7-X probing beam was passing just at the edge of the flat region and, given the placement accuracy of the PEM, may well have been outside of it. However, it is questionable whether the off-axis usage of the PEM in the W7-X interferometer is a significant source for error, given that ρ_c was calibrated to minimize σ_c in this setup. While not shown here, the constellation of the compensated IM did still

exhibit deformations at the center of the PEM aperture for all of the beam cross sections. In conclusion, the PEM position cannot be the primary source for the observed deformations in the constellation.

It should be noted that the LIA-based phase extraction method has a very flat σ_c-curve throughout the entire measurement region. Based on this, it is clear that the PEM position or the gradients of ρ across the beam cross section is not the source for the rotation of the LM's constellation either. The fact that the LM's average corrected σ_c is a factor 3 higher than the corrected σ_c of the IM's curves in the flat region can be attributed to the high levels of noise in these experiments. Since the method is operating far away from the ideal calibration point of ρ, this noise is amplified strongly by the I/Q correction.

In search for another source of PEM-synchronous amplitude modulation, the only obvious choice is the interaction of the PEM with the FDC.

B. FDC alignment error

A quantity that can affect the measured amplitude of a DI is the probing polarization and its interaction with the optics. A DI is a highly polarized system. Not only is the pump beam linearly polarized but also there are several polarization sensitive/active components in the setup. First and foremost, the FDCs themselves define an ordinary (O) and extra-ordinary (X) polarization plane with respect to the pump beam polarization by orientation of their crystal axes. In addition, the phase modulator operates by principle of time-varying birefringence, thus defining its own O and X plane. To see whether the interplay between these different components

is relevant, the same measurement setup described in Sec. IV A was used. The PEM was placed at the probing beam's waist with the beam passing through the center of the PEM's aperture [purple position in Fig. 5(a)]. Laser and PEM were assumed to be aligned by means of their respective housings. The first FDC was rotated around both axes such that the DC diode signal without a second FDC and no phase modulation was maximized. This aligns the crystal axis and the pump beam's polarization vector. The second FDC was rotated around the pump beam propagation axis (z-axis), thus rotating the axis of maximum doubling efficiency away from the pump beam's polarization plane. The matching angle (around the vertical-axis) was slightly adjusted to maximize the diode signal at each rotation step.

Figure 6 shows the results of this investigation. The top plot shows the corrected constellation error σ_c measured by a wedge scan for the IM (thin blue) and the LM (thick orange). The "vertical" (0° mark) is defined by the rotation stage used and differs from the crystal axes due to the nature of the crystal mount. The bottom axes display a few constellation snapshots with the corrections described in Sec. III A applied.

The measurements show that rotation appears to have a profound impact on both methods' constellations. The minimum error (around 7°) is similar for both methods. The same can be said for its gradient going toward negative rotation angles. For positive angles, both methods quickly show significant distortions. The source for this asymmetric behavior could not be fully determined. It is conceivable that the tight aperture of the crystal introduced internal reflections, when rotating it in this direction. However, the fact that the strength and type of distortions seen are similar to the ones seen in the W7-X experimental data, where this was not an issue, indicates
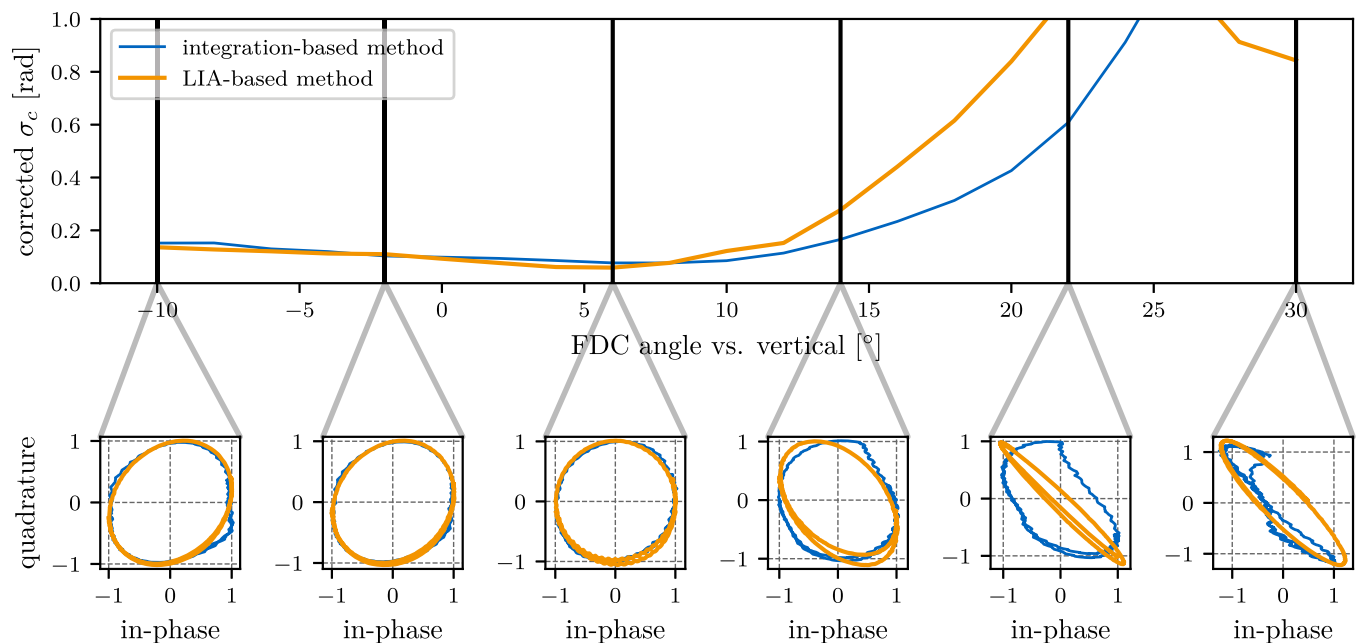
FIG. 6. Constellation errors induced by misalignment of the second FDC for the IM (thin blue) and the LIA-based one (thick orange). The top graph shows the maximum phase error acquired from wedge measurements. The bottom plots show snapshots of the respective constellations with the corrections applied.

that this is an effect originating from the orientation of the crystal axis.

An additional point to note is that the LIA-based error increases significantly faster than the integration-based one for positive FDC rotation angles beyond 8°. As seen from the constellations at the bottom, the LM is strongly affected by the FDC rotation, giving it a higher susceptibility for this source of error.

V. COMPARISON OF METHODS FOR AN EXPERIMENTAL PLASMA DISCHARGE

To compare the simultaneous usage of both phase evaluation methods, the raw data acquired by the integral electron density dispersion interferometer (IEDDI) diagnostic at W7-X was re-evaluated. Figure 7 shows the IEDDI data for the W7-X discharge No. 20171115.22. This was a standard electron cyclotron resonance heated discharge using O2 heating. The base plasma was gas puffed helium. Thirteen hydrogen pellets are being injected from the high field side at around 3.2 s. All thin blue curves in the figure indicate the evaluation using the IM, while the thick orange curves are based on the LIA approach. In both cases, the constellation has the I/Q corrections described in Sec. III A applied. The original constellation is plotted in the background of the top two axes. The constellations in Figs. 7(a) and 7(b) have been decimated. As can be seen from the density trace, the two methods agree very well, albeit a significant deviation can be seen between the 1 and 2 s mark. This is the result of the deviation from an elliptic constellation seen in the integration constellation in Fig. 7(a).

Two regions of interest are relevant here. Figure 7(d) shows an excerpt from the pre-plasma phase, where the IEDDI system should ideally measure zero phase. As can be seen, the IM measures significant changes in the phase although there is no plasma present to induce these. Similar variations have been seen previously, but could not be identified.[6] The LM does exhibit such phase variations, so that an effect based on changes in the optical path length can be excluded. The time scale of these movements is comparatively slow (of the order of 5 ms) and may be the result of changing laser power. The IM appears to be sensitive to the resulting changes in the diode signal amplitude. It should be noted at this point that the high frequency noise in the IM stems from the fact that this method does not filter the output signal; thus, it provides a higher detection bandwidth, which inherently increases noise.

Figure 7(e) is a zoom into one of the pellet injections of the discharge. As can be seen, the two methods disagree on the shape of the density trace. The absolute difference seen is yet again the result of the different constellation shapes. As mentioned in Sec. II, the temporal displacement is the result of the filter employed in the LM, which leads to a phase delay and a smoothed step-response. The IM has no temporal distortions and is accurate down to the level of the digitization clock. More interestingly, the IM reveals features during the ablation phase, which seem to have been strongly filtered away in the LM. As indicated by the coloring, the pellet injection also coincides with a small extrusion from the constellation. While this extrusion hints again at an amplitude induced error, the motion is still moving around the constellation and, thus, is qualitatively correct, even though the absolute value may be shifted.
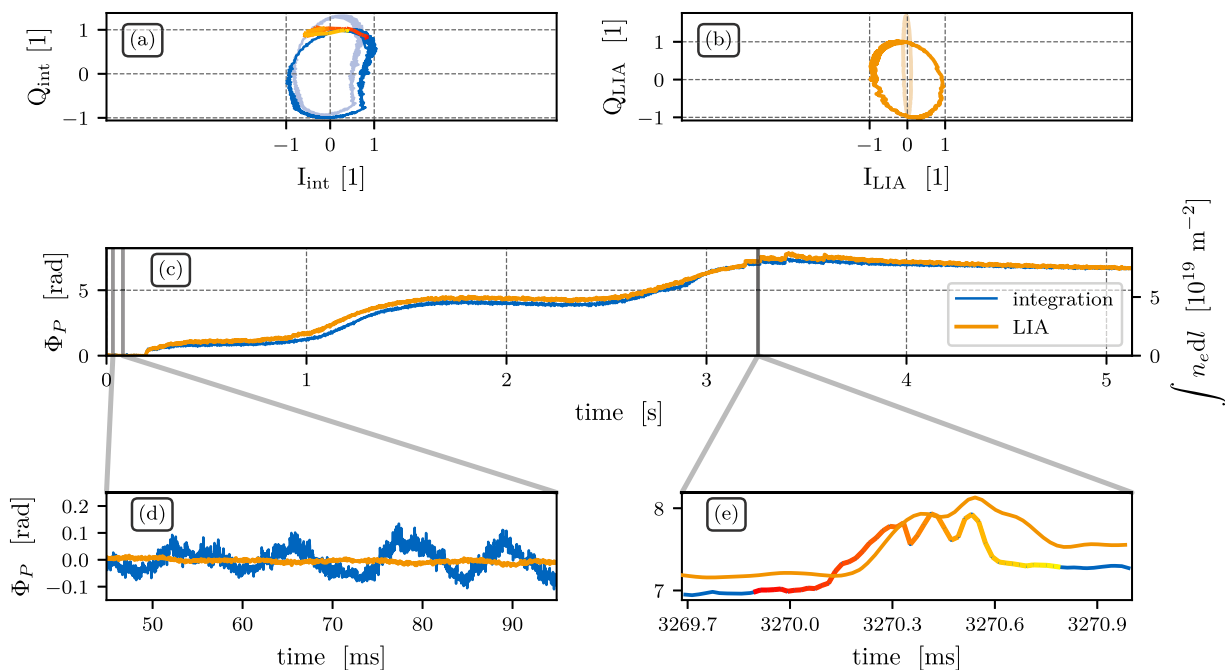
FIG. 7. The density measured by the IEDDI system during W7-X discharge No. 20171115.22 using the IM (thin blue) and the LM (thick orange) is plotted in the middle (c). (a) and (b) show the constellation plot with applied corrections for both methods (the raw constellation is plotted faintly in the background). (d) shows a zoom into the pre-plasma phase. (e) shows the response to a pellet injection. The colored section in (e) marks the correspondingly colored section of the integration constellation in (a).

This is supported by the fact that [opposed to the measurements in Fig. 7(d)] the LIA-method does show washed out features of the pellet ablation.

The final observation to be made from Fig. 7 is the shape of the constellations in Figs. 7(a) and 7(b). The level of distortions seen here are similar to the level of distortions seen in the FDC rotation scan of Fig. 6 around the 14° mark. While this is only a qualitative measure, it indicates that the IEDDI system's constellation errors during the OP1 experimental campaign were the result of a misaligned FDC, which may have been tilted by over 10°.

VI. SUMMARY AND DISCUSSION

We have developed a method to simultaneously use the two dominant phase evaluation methods for modulated dispersion interferometers, where one is based on numerical integration and the other on lock-in amplification. This was possible by implementing an I/Q-correction scheme, allowing to use either method far away from their optimum calibration point. The correction is simple, established, and easily real-time capable. By simultaneously applying both methods to DI phase measurements, a major source for constellation errors could be identified. In addition, the methods could be compared directly in a plasma scenario, revealing advantages and disadvantages for both methods.

Both methods appear to be comparable from an absolute error point of view particularly visible for the scan-angles below 6° in Fig. 6. The LM appears to exhibit smoother distortions, which may be easier to compensate numerically. However, this would require the constellation to remain unchanged. The pellet ablation shown in Fig. 7(e) does show a higher measurement bandwidth and temporal accuracy for the IM, which was originally predicted.[6] However, it also appears to be susceptible to amplitude changes as shown Fig. 7(d).

As such, the IM may be more suitable for high-frequency mode analysis, while the LM is more suitable for low-noise absolute measurement. A direct combination of the two methods is difficult, since the filter response and processing latency differ significantly between the two methods. For the LM, a latency of up to a millisecond is necessary (depending on the implementation and optimization criteria employed), while the IM's latency is two orders of magnitude below that, since no filtering is required.

The combination of the two phase evaluation methods enabled the identification of several sources of systematic errors. The LM does appear to be less affected by non-uniform modulation across the probing beam cross section, as shown in Sec. IV A. However, to the authors' knowledge, W7-X is the only DI currently in operation affected by this type of error. Future DI designs, such as the multi-channel DI planned for W7-X, will have to incorporate this knowledge. In preparation of the OP2 experimental campaign scheduled to start 2022, the modulator of the W7-X IEDDI system will be moved to a different location with a single pass through the center of the aperture. This possible with only minor modifications to the optical design.

A significant source for error was identified in the polarization of the probing beam passing through the second FDC. The distortions seen are evident that the W7-X system was misaligned in the pre-2020 experimental campaigns, since no polarization rotation is expected from the W7-X plasma itself. It could be shown that the constellation error can be removed by alignment of the second FDC. This calibration criterion was never previously considered in modulated dispersion interferometers.

The physical mechanism behind the error could be related to an effect known as "residual amplitude modulation" (RAM) in other fields.[20] In these cases, the misalignment between the modulator and the laser polarization introduces a "swinging" motion of the pump-beam due to the oscillating birefringence in the modulator. When this swinging pump beam is passed to a polarizing element (in this case the FDC), it will introduce an amplitude modulation into the doubled beam. Rotating the crystal in this case will not remove the effect, but will change the phase between the amplitude modulation waveform and the temporal interferogram. With the appropriate phase shift, such a modulation would be mostly corrected by the method outlined in Sec. III A. However, it can be seen that some of the more "elaborate" distortions in the bottom of Fig. 6 cannot be fully removed.

Finally, the simultaneous usage of the two phase evaluation methods identified an amplitude dependence in the IM. The source of this dependence cannot, at present, be determined. A likely origin is the extremum filter employed in the IM. As described in Sec. II, it removes the "static" $I_1 + I_2$ component in Eq. (1). The right hand side of Eq. (1), however, has a DC component attached to it, whose magnitude depends on ϕ_p. Adding a parasitic DC component would create an imbalance in the half-period integrals, which are used for quadrature detection.

However, for the extremum filter to be affected this way, the amplitude variations would have happen on the timescale of the modulation frequency or be synchronous with it. It is conceivable that there is a coupling between the FDC-rotation induced amplitude modulation, which is modulation synchronous and leads to asymmetries in the diode signal, and the extremum filter. This needs to be investigated in the future.

The polarization induced error is a highly significant effect for devices such as ITER and DEMO. In the toroidal interferometers designed for these devices, significant plasma-induced Faraday rotation of the order of 10° to 20° is expected.[21] This rotation will in turn result in systematic errors evolving over the course of a discharge. This is problematic, as the error cannot be distinguished from a phase change due to a plasma on the fly. Since the interferometer is a central control diagnostic also responsible for machine safety, the error directly impacts the safety of the respective fusion device and must therefore be minimized. A potential mitigation scenario is to place the PEM in the outgoing beam before the plasma and using the polarimetric measurement to feed-back on the FDC rotation in real-time.

The experiments conducted in this work were conducted using a ρ calibration point close to the optimum for the IM, which enabled us to draw conclusions from the laboratory experiments to the W7-X plasma experiments. In general, any ρ_c value could have been chosen, since the I/Q-correction would take care of the resulting imbalance for either evaluation method. If one would optimize a real-time processing system for simultaneous usage of both phase evaluation methods, ρ_c should try to balance both method's I/Q ratios while maximizing the smallest of the set of Bessel/Struve functions. A good choice for ρ is 3.15 rad in Fig. 3, which requires roughly the same amount of scaling for both methods while almost maximizing the Bessel/Struve functions.

As a final statement, it must be noted that the investigation here was conducted using AgGaSe$_2$, which is a critically phase matched crystal. The polarization effects shown in Sec. IV B may look very different (or even disappear) using non-critically matched crystals, such as orientation patterned GaAs.[12] Due to their superior doubling efficiency, they are currently envisaged for both ITER and W7-X as a doubling crystal. The experiments in Sec. IV B will be repeated using these crystals to properly qualify the risks for the ITER dispersion interferometer/polarimeter design. Such experiments are already being prepared.

ACKNOWLEDGMENTS

AUTHOR DECLARATIONS

Conflict of Interest

The authors have no conflicts to disclose.

DATA AVAILABILITY

Much of the evaluation in this article was conducted using Python 3.9 in combination with the numpy, matplotlib, and pandas libraries.[22–25]

Raw data were generated at the Wendelstein 7-X facility. Derived data supporting the findings of this study as well as the codes for data evaluation and plot generation are available from the corresponding author upon reasonable request.

REFERENCES

[1] A. Mlynek, G. Schramm, H. Eixenberger, G. Sips, K. McCormick, M. Zilker, K. Behler, J. Eheberg, and A. U. Team, Rev. Sci. Instrum. **81**, 033507 (2010).

[2] A. Boboc, C. Gil, P. Pastor, P. Spuig, T. Edlington, S. Dorling, and J.-E. Contributors, Rev. Sci. Instrum. **83**, 10E341 (2012).

[3] T. Akiyama, R. Yasuhara, K. Kawahata, S. Okajima, and K. Nakayama, Rev. Sci. Instrum. **85**, 11D301 (2014).

[4] H. Sasao, Y. Kawano, H. Arakawa, T. Sakuma, R. Imazawa, H. Kubo, and K. Itami, J. Instrum. **11**, C02082 (2016).

[5] M. A. van Zeeland, T. N. Carlstrom, D. K. Finkenthal, R. L. Boivin, A. Colio, D. Du, A. Gattuso, F. Glass, C. M. Muscatello, R. O'Neill, M. Smiley, J. Vasquez, M. Watkins, D. L. Brower, J. Chen, W. X. Ding, D. Johnson, P. Mauzey, M. Perry, C. Watts, and R. Wood, Plasma Phys. Controlled Fusion **59**, 125005 (2017).

[6] K. J. Brunner, T. Akiyama, M. Hirsch, J. Knauer, P. Kornejew, B. Kursinski, H. Laqua, J. Meineke, H. Trimiño Mora, and R. C. Wolf, J. Instrum. **13**, P09002 (2018).

[7] Y. F. Wang, H. Q. Liu, Y. X. Jie, H. Lian, Y. Q. Chu, W. M. Li, S. X. Wang, and X. Zhu, J. Instrum. **15**, T06009 (2020).

[8] M. A. van Zeeland, R. L. Boivin, D. L. Brower, T. N. Carlstrom, J. A. Chavez, W. X. Ding, R. Feder, D. Johnson, L. Lin, R. C. O'Neill, and C. Watts, Rev. Sci. Instrum. **84**, 043501 (2013).

[9] W. Biel, R. Albanese, R. Ambrosino, M. Ariola, M. V. Berkel, I. Bolshakova, K. J. Brunner, R. Cavazzana, M. Cecconello, S. Conroy, A. Dinklage, I. Duran, R. Dux, T. Eade, S. Entler, G. Ericsson, E. Fable, D. Farina, L. Figini, C. Finotti, T. Franke, L. Giacomelli, L. Giannone, W. Gonzalez, A. Hjalmarsson, M. Hron, F. Janky, A. Kallenbach, J. Kogoj, R. König, O. Kudlacek, R. Luis, A. Malaquias, O. Marchuk, G. Marchiori, G. Mattei, F. Maviglia, G. De Masi, D. Mazon, H. Meister, K. Meyer, D. Micheletti, S. Nowak, C. Piron, A. Pironti, N. Rispoli, V. Rohde, G. Sergienko, S. El Shawish, M. Siccinio, A. Silva, F. da Silva, C. Sozzi, M. Tardocchi, M. Tokar, W. Treutterer, and H. Zohm, Fusion Eng. Des. **146**, 465 (2019).

[10] T. Akiyama, M. A. V. Zeeland, T. N. Carlstrom, R. L. Boivin, K. J. Brunner, J. Knauer, R. Yasuhara, K. Tanaka, H. Q. Liu, Y. Zhou, N. Oyama, A. Sirinelli, K. Urabe, and N. Shirai, J. Instrum. **15**, C01004 (2020).

[11] S. Moon, P. Petersson, M. Rubel, E. Fortuna-Zalesna, A. Widdowson, S. Jachmich, A. Litnovsky, and E. Alves, Nucl. Mater. Energy **19**, 59 (2019).

[12] K. Termkoa, "Development of orientation-patterned gallium arsenide and gallium phosphide templates using wafer fusion for frequency doubling applications," Ph.D. thesis, University of Massachusetts Lowell, 2010, copyright—Database copyright ProQuest LLC; ProQuest does not claim copyright in the individual underlying works, last updated—November 23, 2020.

[13] T. Akiyama, K. Kawahata, S. Okajima, and K. Nakayama, Plasma Fusion Res. **5**, S1041 (2010).

[14] P. A. Bagryansky, A. D. Khilchenko, A. N. Kvashnin, A. A. Lizunov, R. V. Voskoboynikov, A. L. Solomakhin, and H. R. Koslowski, Rev. Sci. Instrum. **77**, 053501 (2006).

[15] S. Bhattacharyya, R. N. Ahmed, B. B. Purkayastha, and K. Bhattacharyya, J. Phys.: Conf. Ser. **759**, 012096 (2016).

[16] T. Abeyasekera, C. M. Johnson, D. J. Atkinson, and M. Armstrong, IEEE Trans. Power Electron. **18**, 1315 (2003).

[17] G. Xing, M. Shen, and H. Liu, IEEE Trans. Wireless Commun. **4**, 673 (2005).

[18] G. C. Catella and D. Burlage, MRS Bull. **23**, 28 (1998).

[19] B. Wang and J. List, Proc. SPIE **5888**, 58881I (2005).

[20] Y. Yu, Y. Wang, and J. R. Pratt, Rev. Sci. Instrum. **87**, 033101 (2016).

[21] M. van Zeeland and C. Watts, TIP chit 11—Accuracy of the polarimeter system [6662JN], Technical Report No. ITER_D_7M37ZJ, ITER, 2012.

[22] Python Software Foundation, Python, https://www.python.org, 2001.

[23] W. McKinney, in Proceedings of the 9th Python in Science Conference, edited by S. van der Walt and J. Millman (SciPy Conferences, 2010), pp. 51–61.

[24] J. D. Hunter, Comput. Sci. Eng. **9**, 90 (2007).

[25] S. van der Walt, S. C. Colbert, and G. Varoquaux, Comput. Sci. Eng. **13**, 22 (2011).